Separating the effects of wall-blocking and near-wall shear in the interaction between the wall and the free shear layer in a wall jet

A. Dejoan and M.A. Leschziner
Department of Aeronautics, Imperial College London,
London SW7 1AZ, UK.
Email: a.dejoan@imperial.ac.uk, mike.leschziner@imperial.ac.uk

Abstract

The statistical and structural characteristics of two plane jets, one developing along a real wall and the other along a frictionless wall (equivalent to a zero-shear, non-deformable free surface) are compared by way of highly-resolved LES solutions at computational conditions close to those of DNS. The aim is to distinguish between two types of influence of the wall on the outer shear layer: one inviscid, arising from wall blocking, and the other, associated with the near-wall shear in the boundary layer. Results are presented for mean-flow properties, second moments and budgets thereof, structural characteristics and the integral length scale. The comparisons demonstrate that the wall affects a significant proportion of the outer shear layer to a depth of approximately 3 times the thickness of the boundary layer, with or without wall shear. Outside the immediate near-wall layer, in the interaction region, the influence of the wall is effected by an interplay between turbulence diffusion towards the wall and inviscid processes associated with pressure fluctuations and their reflection from the wall. The addition of shear modifies substantially the statistical behaviour and structure within the thin sheared region. The state of anisotropy and the energy-redistribution process among the normal-stress components change drastically, the structure is dominated by small scale, elongated eddies, and the near-wall layer is observed to "shield" the wall from the penetration of large-scale vortices from the outer shear layer. The role of diffusion, in particular, renders the near-wall shear layer very different from a conventional equilibrium boundary layer, its integral scale being considerably enhanced by the influence of large-scale eddies originating in the outer shear layer and migrating towards the wall.

1 Introduction

The processes by which a free shear layer — say, one that evolves following separation — interacts with a near-wall layer adjacent to it, across an “overlap” region, can have a significant impact on the gross behaviour of the flow containing these shear layers. Examples in which such an interaction occurs are separated flows recovering from reattachment, wall jets injected into an ambient flow in the context of wall cooling or separation control, and impinging jets used to enhance heat transfer or arising in VSTOL aircraft operation.

From a fundamental point of view, the interaction can lead to a substantial modification of both component flows – for example, by the penetration or “migration” of disparate turbulent scales from one shear layer to the other. This process can have significant implications for the rate of mixing of the flow as a whole and the turbulence structure within it. It is important, therefore, to understand the fundamental mechanisms involved, both as an end in itself and as a foundation for developing improved statistical closures for such flows.

Modelling post-reattachment recovery is a case in point: it is often observed that turbulence closures that predict correctly the separated zone, including the reattachment point, underestimate the rate of recovery. In this region, the turbulence structure of the flow departs substantially from the equilibrium conditions that are used to formulate and calibrate models for near-wall shear flows. This lack of equilibrium is not merely due to upstream history, but also linked to cross-stream transport that is driven by the disparity of the constituent layers that form the post-reattachment wake. A recent study by Dejoan and Leschziner [1] provides compelling evidence that the interaction mechanisms considered herein are highly pertinent to the near-wall layer in both separated and post-reattachment regions.

The simplest flow that features the type of interactions considered above is the (statistically) two-dimensional, plane wall jet. This consists of an outer, separated shear layer and an inner boundary layer, which “communicate” across an “overlap” region. Recent highly-resolved LES studies by the present authors [2], [3] have highlighted some influential mechanisms specific to the interaction between the two shear layers – in particular, the influence of turbulent-stress diffusion across the overlap region and the migration of large-scale eddies from the outer to the inner flow. Taking advantage of the data generated for the wall jet, a recent study by the present authors (Dejoan *et al.* [4]) investigates, by way of *a-priori* examinations as well as model calculations, the validity of a variety of second-moment-closure approximations for the wall jet, and demonstrates a rather poor representation by the models of stress diffusion and pressure-velocity interaction.

An interesting question that arises in relation to the behaviour of the wall jet or any other wall-affected set of shear layers is what the relative contributions of near-wall shear and the inviscid wall-blocking are to the observed interaction across the overlap region. In the context of statistical modelling, this question is of interest in efforts to devise improved second-moment-closure models, particularly in the case of models in which the anisotropy due to shear and wall-blocking are approximated by separate closure fragments. The two contributions may be investigated by comparing the flow in a realistic wall jet with one in which the wall is treated as being shear-free. While in both flows, wall-blocking causes the wall-normal fluctuations to decline, an obvious difference is that the tangential fluctuations decay to zero only in the presence of the real wall.

Early studies of wall-blocking effects, separated from the influence of wall-shear, were pursued by considering the near-wall behaviour of decaying grid turbulence in a uniform stream bounded by a wall that moves at the same mean speed as that of the stream. In a conceptual model proposed by Hunt and Graham [5], two distinct boundary layers are identified near the wall: an inner viscous layer and an outer “source” layer, the former embedded in the latter and its influence depending on the Reynolds number, based on turbulence energy and its rate of dissipation. At low values, the inner viscous layer is held to dominate the source layer, and turbulence is damped close to the wall; in contrast, at high values, the source layer dominates and the turbulence intensity parallel to the wall increases as the rigid wall is approached. This model reconciles the near-wall damping observed in the experiments of Uzcan and Reynolds [6] and the increase in turbulence observed by Thomas and Hancock [7] at higher Reynolds numbers. A subsequent LES study by Biringer and Reynolds [8] confirmed the validity of Hunt's and Graham's proposition. An important process predicted by the model of Hunt and Graham, recently confirmed by the experiments of Aronson *et al.* [9] as well as the DNS of Perot and Moin [10], is an energy transfer in the source layer from the "low-energy" wall-normal component to the "high-energy" wall-parallel components. The source layer thus originates from the shear-free near-wall layer, subjected to the impermeability condition, and its thickness is roughly the size of the macro length scale of the free-stream turbulence. To gain further insight into the influence of the wall, Perot and Moin considered different types of boundary: an idealized permeable wall, to isolate the viscous and shear effects, an idealized free surface, to allow the kinematic effects to be isolated, and finally a no-slip wall at which both viscous and kinematic effects occurred simultaneously. They show that the nature of the inter-component energy transfer near the surface/wall is associated with an imbalance between "splats" and "anti-splats", the level being controlled by viscous processes - i.e. dissipation and diffusion.

Other studies pertinent to the present subject deal with the interaction of shear-layer turbulence with a free surface, some idealizing it as a rigid free-slip wall. The DNS of open channel flow performed by Handler *et al.* [11], Rashidi and Banarjee [12], Lam and Banarjee [13] and Pam and Banarjee [14] analyse the interaction between structures originating from the bottom wall of open-channel flow and migrating towards the opposite free-slip surface. Handler *et al.* report Reynolds-stress budgets which indicate, as observed in grid turbulence next to a moving wall, an energy transfer from the wall-normal component to the horizontal ones near the free surface. They also propose a "pancake" model to explain the increase of the horizontal length scales and the decrease of vertical scales they observe. Banarjee and his co-authors give details on the near-surface structural features of turbulence, identifying quasi-two-dimensional, persistent large-scale structures. They also consider the effect of mean shear superimposed at the free surface (induced, say, by wind shear) and show that streaky structures can form at the free surface when the shear is high enough. A similar result was also obtained by Kuroda *et al.* [15] in their DNS of turbulent plane Couette-Poiseuille flows. A further, more recent, numerical study that focuses on the development of a turbulent shear flow with imposed strain under a free surface is that of Shen *et al.* [16]. Reynolds-stress budgets are reported and a structural analysis is provided, including Froude-number effects. A thin "surface layer" and a "blockage layer" below it are identified, the latter corresponding to the outer "source layer" mentioned earlier in relation to decaying grid turbulence, while the former is characterised by a sharp decrease of the tangential stresses over a very thin region near the free surface, caused by the imposed zero-stress conditions. The study shows that the reduction of the vertical-velocity fluctuations occurs without any appreciable increase in turbulence-energy dissipation as the wall is approached, but is, as observed earlier, primarily compensated by an increase in the horizontal velocity fluctuations.

While the studies reviewed above highlight the fundamental nature and consequences of the energy-transfer mechanism provoked by wall blocking, and shed some light on the effects arising from the presence of near-wall shear, they do not characterize the details of the interaction between an intensely strained, free shear layer in close proximity with a wall, thus being subjected to the combined action of blocking and shear on its near-wall side. The present study contributed to bridging this gap. This is done through the use of highly-resolved large eddy simulations to study the interaction between an outer shear layer of a jet flow, characterized by large-scale motions and high turbulence intensity, and two types of wall: a no-slip wall and an impermeable zero-shear plane. The latter can be viewed as a free, non-deforming liquid surface in the limit of zero Froude number. The absence of wall shear prevents the formation of wall turbulence and drastically modifies the interaction between the large-scale eddies contained in the outer layer and the near-wall region, relative to a conventional wall jet. Extensive statistical data are presented, among them budgets for the Reynolds stresses and turbulence energy. These permit the details of the interaction to be analyzed as a preliminary to the study of statistical models based on second-moment closure, pursued by the present authors in reference [4]. Particular attention is devoted to the energy-redistribution process through the non-deviatoric part of the pressure-velocity correlation. In addition, length scales are extracted, and these illustrate, among others, that the interaction results in strong departures from turbulence equilibrium, the condition that usually characterises the constituent shear layers when these exist in isolation. To supplement the above statistical information, some structural visualisations are included. These provide valuable qualitative indicators to the nature of the instantaneous processes that give rise to particular aspects of the statistical behaviour.

2 The flows and the approach to their simulation

In both geometries, the jet is injected at the velocity U_o through a slot of height b in a vertical wall (see Fig. 1). The Reynolds number, $R_e = U_o b/\nu$, is 9600. The size of the domain is $22b \times 10b \times 5.5b$ in the streamwise, transverse and spanwise directions, respectively. The choice of this domain is based on experimental observations by Eriksson *et al.*, [17] [18], for the same conditions as simulated here (with the no-slip state imposed at the wall), indicating that the flow essentially reaches a self-similar state when the flow reaches a streamwise distance of about 20 jet heights. At the inflow, $x/b = 0$, the time-mean velocity and turbulence-intensity profiles were extracted from the experimental conditions. The inlet flow is effectively laminar, with the measured low level of fluctuations therein represented by superposing weak random perturbations onto the mean inlet flow. At the outflow, $x/b = 22$, a convective, non-reflective boundary condition was applied (see Dejoan and Leschziner, [2]). At the upper boundary, $y/b = 10$, a distribution of entrainment velocity, determined from the theoretical solution given by Schlichting [19], not exceeding 5% of the velocity U_o was prescribed. At the lower boundary, no-slip conditions were applied in the case of the wall jet, while the conditions at the shear-free wall were prescribed as a combination of impermeability and zero-wall-normal gradients of the wall-parallel velocity components.

The numerical grid contains 420x208x96 (8.4 million) nodes, and was carefully chosen so as to give very low subgrid-scale contributions, approximated with Germano's dynamic Smagorinsky model (Germano *et al.* [20]). The choice of this particular model was judged appropriate because of the transitional character of the flow within the initial 5 jet heights. While this is of little significance to the properties of the flow in the self-similar region – that of primary interest in this study – it does affect the initial evolution of the flow, albeit weakly. Fig. 2 shows the ratio of the cell size, Δ, to the Kolmogorov length, $\eta = \nu^{3/4}\varepsilon^{-1/4}$, to be, typically, 5-10. These distributions were determined using data for the rate of dissipation, ε, derived from the balance of all other contributions to the turbulence-energy budget (see eq. 1). Consistent with the above are the observations that the time-mean subgrid-scale viscosity is of the order 0.5 times the fluid viscosity, and that the dissipation rate extracted explicitly from the simulation is about 70% of that determined from the balance (see Fig. 16). Moreover, the spectra shown in Fig. 3 demonstrate the spectral cut-off to lie in the dissipative range. In the outer shear layer, the wall-normal grid distance ranges from $\Delta y/b = 0.02$ to 0.05 in the region $1 < y/b < 5$. In the near-wall layer, the region $0 < y/b < 1$ is covered by 100 nodes. In the wall jet, the near-wall cell-aspect ratio is, typically, $\Delta y^+/\Delta x^+/\Delta z^+ = 1.2/24/24$, the wall-nearest grid node lying at $y^+ = 0.6$. Statistical results, presented in the next section, were obtained by integrating the solution over 20 and 26 flow-through times for the real jet and shear-free-wall jet, respectively, the longer integration time for the latter necessitated by the more pronounced presence and persistence of long-time-scales eddies in the outer part of the shear layer. The computational method is a general multi-block, finite-volume scheme incorporating second-order discretisation in space and time. Time-marching is based on a fractional-step and projection method. The code is fully parallelised and was run on up to 512 ORIGIN 3800 processors. More details on the simulation parameters can be found in Dejoan and Leschziner [2].

3 Results

3.1 Introductory considerations

When examining the wall jet on its own, by reference to measurements of Eriksson *et al.* [17] [18], Dejoan and Leschziner [2] [3] present comparisons in inner, outer and mixed scaling. Here, comparisons are only possible in terms of quantities normalised by the outer scales U_{max} and $y_{1/2}$, the distance from the wall to the half-of-maximum-velocity point (see Fig. 1). With this scaling, the outer layers in both flows examined here exhibit a self-similar behaviour far downstream of the inlet. Thus, comparisons between the two flows can be made, at least in the outer layer, without reference to the streamwise evolution of the flows.

In what follows below, profiles of mean and turbulence properties as well as budgets are given for the location $x/b = 20$, at which both flows are close to being in a self-similar state. Fig. 1 illustrates the streamwise evolution of the real wall jet through contours of an instantaneous velocity field in one spanwise plane. This shows that transition in the outer shear layer occurs at around x/b=2, while turbulence is observed to be fully established at the location $x/b \sim 12$. A similar behaviour has been observed for the zero-wall-shear jet.

3.2 Mean-flow and second moments

The mean-flow characteristics of the two jets are compared in Figs. 4 and 5 by way of distributions for the decay of maximum velocity, the spreading rate and mean-velocity components at $x/b = 20$. The comparisons show that the maximum streamwise velocity of the real wall jet decays faster – an expected behaviour – because of the loss of momentum induced by the wall-shear stress. However, the spreading rates are close, that of the wall jet being slightly lower, at $dy_{1/2}/dx = 0.073$, than the value for the zero-wall-shear jet, at $dy_{1/2}/dx = 0.076$ (the linear extension of the spreading rate in Fig. 4 beyond the end of the computational domain $x/b = 22$ is intended to accentuate the difference). The very similar slope of the spreading rate obtained for both flows suggests that the reduction of the spreading rate of both jets examined herein relative to a free jet is mainly a consequence of wall-blocking, which reduces the wall-normal fluctuations and hence the shear stress, the latter directly affecting the turbulence production in the near-wall portion of the outer layer.

The mean-velocity profiles, contrasted in Fig. 5, are seen to be fairly similar to each other, except for U near the wall. In the zero-wall-shear case, the velocity U appears not to approach asymptotically the expected zero-gradient condition at the wall. However, Fig. 6 shows, by way of the near-surface variation of the strain $\partial\overline{U}/\partial y$, that the gradient decreases sharply very close to the wall, and that it does reduce to zero at the wall itself. A very similar profile is reported by Shen *et al.* (Fig. 6 in [16]), based on their DNS of a turbulent shear flow under a free surface, and these authors refer to the high strain region as a "surface layer", caused by the dynamic boundary condition that requires a vanishing tangential stress at the free surface. In the presence of wall shear, a thin boundary layer is present. The variation of the strain in this region, not included herein, indicates the thickness of this layer to be close to $0.05y/y_{1/2}$. A noteworthy difference between the two profiles in Fig. 5 is that the non-dimensional shear strain in the outer shear layer is lower in the absence of wall shear. This may be taken to imply a higher level of cross-flow turbulent diffusion. Indeed, as will be shown below, the shear stress is higher in the zero-wall-shear jet.

Figure 5 shows that the wall-normal velocity profiles are very similar in the wall region for both flows. This suggests that wall-blocking, which is a consequence of the kinematic boundary condition and present in both jets, affects the wall-normal component in both cases to a similar extent. However, as will be shown below, the influence of the impermeability condition manifests itself differently when the turbulence statistics of the two jets are contrasted.

Results for the second moments are presented in four ways, each bringing to light different features that enhance the overall view of the differences between and common features of the two jets. First, profiles of the Reynolds-stress components at $x/b = 20$ are given in Fig. 7. Second, distributions of the normal components of the anisotropy tensor $b_{ij} = \overline{u_i u_j}/2k - 1/3\delta_{ij}$ are given in Fig. 8. Third, in the same figure, a scalar measure or norm of the anisotropy is conveyed via the so-called "flatness parameter", A, defined as $A = 1 - 9/8(II - III)$, where $II = b_{ij}b_{ij}$ and $III = b_{ij}b_{jk}b_{kj}$ are, respectively, the second and third invariants of the isotropy tensor. This parameter has been shown by Lumley to vary between 1 for isotropic turbulence and 0 for two-component turbulence at a wall. Finally, Fig. 9 shows variations of the anisotropy across the two jets as loci within the so-called realisability (or Lumley) maps, which co-relate the second and the third stress invariants.

As regards the Reynolds-stress profiles, the most prominent differences between the two cases are, first, the finite value of the turbulence energy at the shear-free wall, and second, the sign reversal in the near-wall shear stress in the real jet, associated with the sign reversal in the shear strain (the two reversals occurring at different locations, however, for reasons discussed by Dejoan and Leschziner[2]). The former is obviously a consequence of the impingement of the turbulent motions originating in the outer layer turbulent on the wall, coupled with the absence of a viscous near-wall layer, which, in the real jet, fully damps the turbulent fluctuations at the wall itself. In the boundary layer, the three normal-stress components vanish, whereas, at the shear-free wall, only the wall-normal stress does so.

A key feature that differentiates the two flows is the turbulence generated by the high level of wall shear in the real jet, relative to (nearly) zero production in the zero-wall-shear jet. This production process is directly associated with the near-wall peak in the streamwise stress, $\overline{uu}$. In contrast, the rise in this stress in the absence of wall shear is, as will transpire from the budgets, a consequence of energy being transferred from $\overline{vv}$ to $\overline{uu}$ and $\overline{ww}$. As the shear-free wall is approached, $\overline{uu}$ and $\overline{ww}$ increase over a very thin region, which corresponds to the surface layer in which the mean shear decreases sharply (see Fig. 6). At the wall, the horizontal stresses almost reach the same value, reflecting a broadly symmetric redistribution of energy from $\overline{vv}$ to the wall-parallel components. A similar increase of the wall-parallel stresses over the thin surface layer is observed in Shen *et al.*. For this region, Shen *et al.* discuss the structural processes and show that, inside the surface layer, vortex structures are swept towards the wall. These "splat" events are the main cause of the sharp increase in $\overline{uu}$ and $\overline{ww}$. The next section illustrates some of the near-wall structural features in the present flows. In particular, it will be shown that, in the absence of wall-shear, intense impingement events of large-scale eddies emerging from the outer layer of the jet occur in the near-wall region (see Fig. 12).

In the real jet, the inter-component energy transfer noted above is also effective, as verified later in section 3.5, but is different in character, due to the wall-shear-induced turbulence production. In this case, the increase of the component $\overline{uu}$ due to the wall shear is such that energy from $\overline{uu}$ has to be transferred to the spanwise component $\overline{ww}$. This redistribution process is associated with the minor near-wall peak of $\overline{ww}$. However, the intensity level of the spanwise stress $\overline{ww}$ is lower than $\overline{uu}$, because only the latter is driven by shear-induced production.

By reference to the $\overline{vv}$ profile (Fig. 7), the "blockage" layer over which the normal stress is damped appears to be thicker in the presence of wall shear. Thus, in the absence of wall shear, $\overline{vv}$ starts to be damped at the distance $y/y_{1/2} \sim 0.5$ from the wall, while in the real jet damping begins at $y/y_{1/2} \sim 0.75$. For both flows, the thickness of the "blockage" layer, deduced from the $\overline{vv}$ profiles, is of the order of the macro scale, $y_{1/2}$, representative of the thickness of the outer free shear layer, an observation that is in accord with previous work (see [16]). However, an examination of the budgets, in particular an analysis of the contributions that are associated with the redistribution of the turbulence energy, leads to a more conservative estimate of the thickness of the "blockage" layer, and this is discussed in Section 3.5.

A general conclusion derived from Fig. 7 is that, in absence of wall-shear, the turbulence activity is amplified, not only in the vicinity of the wall, but also across much of the outer shear layer. This is a potentially important observation, for it suggests that effects arising from the viscous, sheared nature of the near-wall layer extend well beyond this layer, across a major proportion of the whole flow, possibly reflecting effects emanating from the substantial structural differences in the turbulence fields highlighted above. As will be shown later, the structural differences across the flow are also reflected by major differences in the integral length scale in the two flows and by differences in the behaviour of the anisotropy invariants.

A more differentiated view of the effects of near-wall shear on the anisotropy is gained from Fig. 7, which shows the anisotropy among the normal stresses, expressed by $b_{ii} = \overline{u_i u_i}/k - 2/3$ (no summation on i), and by the associated flatness parameter A, defined earlier. The focus on A, rather than on the invariants II and III separately, reflects the fact that, in the context of RANS modelling, A is often used to procure the appropriate sensitivity of the pressure-strain approximation and dissipation equation to the proximity of the wall.

In the real jet, the near-wall variations of b_{ii} are similar, in principle, to those found in a standard boundary, with a high level of anisotropy in the wall-parallel components, $b_{11} > b_{33}$, evidently associated with the near-wall shear production that only contributes to the streamwise component $\overline{uu}$. As will be shown later, by reference to the budgets, a loss of energy from $\overline{uu}$ and its transfer to $\overline{ww}$ results in a weakening of this anisotropy. Hence, the degree of the disparity between b_{11} and b_{33} is not simply dictated by shear production, but involves other influential processes. In contrast, in the absence of wall shear, the profiles of the wall-parallel components of the anisotropy tensor are close, and the wall-parallel isotropy components are almost identical at the wall. Further away from the wall, the influence of the outer shear layer tends to enhance the streamwise component b_{11}. The component b_{22} is hardly sensitive to the presence or absence of wall shear, and its decline therefore reflects almost entirely the wall-blocking process. Interestingly, the distributions of the flatness parameter A approach zero in a broadly similar fashion, suggesting that wall-blocking - that is, the strong disparity between b_{22} and the two other components - is the dominant contributor to A. The presence or absence of shear is identified, albeit rather weakly, by differences in the distance over which wall-blocking is effective. This thickness is of the order $y/y_{1/2} \sim 0.1$ and $y/y_{1/2} \sim 0.15$ for the zero-wall-shear and real jets, respectively. A more detailed analysis of the processes by which the near-wall stresses are affected by the wall, based on a consideration of the redistribution of turbulence energy by the pressure-velocity interaction process, will be given below in Section 3.5.

An alternative view of the anisotropy across the two jets is conveyed in Fig. 9 via loci within the so-called realisability (or Lumley) maps, which co-relate the second and the third stress invariants. Free shear layers are known to exhibit loci that are broadly aligned with the lower, left-hand line of the triangular domain, characterising "axisymmetric expansion". This is a behaviour returned by the zero-wall-shear jet. As the shear-free wall is approached, turbulence tend to a two-component state (as $\overline{vv}$ declines rapidly). This state is identified by the upper side of the triangle. In the presence of wall shear, there is a tendency for II and III to move upwards, broadly parallel to the lower right-hand line of the triangle. This is a behaviour characteristic of near-wall shear. In fact, in a conventional boundary layer, the state of anisotropy in the log-law region is characterised by a locus hugging the lower right-hand-side line. Thus, the real wall jet features a thin near-wall region that is akin to a log-law layer. However, the mean-velocity profile for the wall jet, reported in Dejoan and Leschziner [2], shows that this log layer is thin and indistinct, reflecting the strong influence of the outer shear layer on the near-wall region.

3.3 The near-wall flow structure

In any wall-bounded flow, the near-wall structure is characterized by longitudinal "streaks" associated with high- and low-speeds streamwise fluid motions. However, the studies of Lee *et al.* [21], Lam and Banarjee [12], [13] and Kuroda *et al.* [15] suggest that the formation of such streaks is not closely tied to the presence of the physical wall itself, but is a consequence of high shear. This is exemplified by their respective numerical studies on the application of a uniform shear and of a mean shear onto a free-slip surface, which yield, at sufficiently high shear, a streaky structure characteristic of that near a wall. Conversely, when shear is absent at the free-slip surface, no streaks are observed close to the surface.

The present results confirm these observations. In the near-wall region of the real jet, the instantaneous contours of the streamwise-velocity fluctuations, presented on Fig. 10, exhibit fine and elongated patterns associated with streaks. In contrast, the field of streamwise-velocity fluctuations at the surface of the zero-wall-shear jet is characterised by much more "isotropic" (pancake-like) structures that would be expected to form by the "splatting" of eddies without preferential wall-parallel orientation. However, in both jets, well beyond the near-wall shear layer, the flow structure is very similar in both jets, as is illustrated by Fig. 11. Splatting is well conveyed by Fig. 12, which shows instantaneous fields of the transverse $(w/U_o, v/U_o)$ fluctuating velocity. In the absence of wall shear, strong impinging motions, exemplified by the "splat" in the figure, are accompanied by ejections, exemplified by the "anti-splat". In presence of wall-shear, the fluid motions are damped very near the wall due to viscous effects, resulting in a far less intense turbulence activity. The persistence of near-wall streaks in the presence of large, energetic eddies contained in the outer layer and continuously migrating towards the wall suggests a robustness of the streaky near-wall structure, whatever the turbulence intensity of the outer layer is. Similar structural properties were also observed by Jimenez and Pinelli [22] in a channel flow in which the turbulence energy in the core of the channel was artificially damped, and this led Jimenez and Pinelli [22] to argue the existence of an autonomous wall cycle that is largely divorced from the outer flow.

Instantaneous iso-contours of the streamwise vorticity, bW_x/U_o, across a near-wall portion of the $y-z$ plane are shown in Fig. 13. The contours indicate the presence of large-scale eddies in the wall region of the zero-wall-shear jet. These large scale eddies, issued from the outer layer, reach the wall without evident attenuation of their length scale, as illustrated by the structures around the spanwise locations $z/y_{1/2} = 0.1$ and $z/y_{1/2} = 0.3$, and suggested by Figs. 10 and 11. In contrast, the near-wall region of the real jet is populated with small-scale eddies, especially very close to the wall $y/y_{1/2} < 0.01$ (corresponding to $y^+ < 10$ in terms of wall coordinates based on the friction velocity of the real jet), which are characteristic of any near-wall shear layer. These near-wall eddies inhibit a direct contact of the larger-scale eddies originating from the outer layer with the wall, and may be viewed as forming a thin layer of small-scale eddies slightly flattened by the splatting of the outer eddies. Animations reveal that the small wall eddies tend to continuously merge (or mix) with the larger eddies.

The structural differences are reflected by related features in specific statistical parameters, some already highlighted in the previous section in terms of second moments. Here, skewness and flatness (Kurtosis) profiles are presented on Figs. 14-15 for both the real and zero-wall-shear jets. These give information about the shape of the probability density functions of the velocity components, specifically on the bias of fluctuations towards negative or positive values. For perfectly Gaussian p.d.f's, the skewness is zero and the flatness is 3. As seen, this applies, broadly, to both jets beyond the near-wall region $y/y_{1/2} > 0.05$. In the case of the real wall jet, the positive peaks of the skewness of the streamwise and wall-normal stresses, S_u and S_v, also observed in a standard boundary layer, reflect the low- and high speed streak fluid motions associated with the wall cycle of burst and sweeps events.

When the wall shear is suppressed, the skewness S_v features a strongly negative peak value at the surface, which suggests, in contrast to the real jet, strong motions towards the wall, consonant with the splatting paradigm. At the free surface, S_u and S_w are very low, which is consistent with the observation of non-preferential "splatting" noted above by reference to Fig. 10.

The flatness distributions for the two jets are broadly similar, but differ in detail. The wall peak in F_v is indicative of a highly skewed p.d.f. characterised of a state of intermittency associated with the streaky wall structure in the real jet and with splat and anti-splat events in the zero-wall-shear jet. In the case of the zero-wall-shear jet, the near-wall values of F_u and F_w remain close to 3, and this is consistent with the near-Gaussian p.d.f's already identified by reference to the near-zero levels of the skewness. Thus, the behaviour of these two components is dictated by the structure of eddies remote from the wall, which migrate towards the wall and splat onto it without being subjected to viscous damping - a process increasing intermittency in the wall-normal direction. In the real jet, F_u and F_w exhibit peak values at the wall, characteristic of the shear-produced turbulence structure near the wall seen in Fig. 10.

3.4 Budgets

This section presents budgets for the turbulence energy and the Reynolds-stress components extracted by reference to the second-moment equations (1):

$$
\begin{aligned}
\frac{\partial \overline{u_i u_j}}{\partial t} + \underbrace{\overline{U}_k \overline{u_i u_j}_{,k}}_{C_{ij}} &= \underbrace{-\overline{u_k u_j} U_{i,k} - \overline{u_k u_i}\overline{U}_{j,k}}_{P_{ij}} \\
&+ \underbrace{\nu \overline{u_i u_j}_{,kk}}_{D_\nu} \underbrace{-\overline{u_i u_j u_k}_{,k}}_{TTT_{ij}} \underbrace{-\frac{(\overline{u_i p_{,j}} + \overline{u_j p_{,i}})}{\rho}}_{\Pi_{ij}} \\
&\underbrace{\underbrace{-2\nu \overline{u_{i,k} u_{j,k}}}_{\varepsilon_{c_{ij}}} + \text{SGS terms}}_{\text{balance}=\varepsilon_{ij}}
\end{aligned} \tag{1}
$$

Attention is drawn to the fact that the dissipation rate reported in the budgets to follow is not computed explicitly from the filtered field, denoted by $\varepsilon_{c_{ij}}$ above, but from the balance of all other processes, ε_{ij}, as indicated in Eqs. (1). The balance ε_{ij} thus represents the total level of dissipation, including the viscous and subgrid-scale parts, denoted by "SGS terms" in (1). As noted earlier, the level of resolution is such that the computed turbulence-energy dissipation ε_c is typically 70% of the level deduced from the balance, ε_k (see Fig. 16). More details on resolution issues can be found in Dejoan and Leschziner [2].

Corresponding budgets for the turbulence energy and the Reynolds stresses in the outer, wall-remote layer differ little between the two jets or indeed from any other free shear layer. This is illustrated in Fig. 16 by reference to the turbulence energy. It is therefore of limited interest to examine this region in detail, and budgets for the individual stress components covering the outer layer are omitted. Rather, attention focuses in what follows on the near-wall region and the interaction zone $0 < y/y_{1/2} < 0.5$, to which the budgets presented in Figs. 17 to 21 appertain.

The near-wall budgets, given in Figs. 17 to 21, indicate substantial differences between the two flows. The most important agency for these differences is the shear-induced generation at the wall, which directly affects k, $\overline{uu}$ and $\overline{uv}$. In the first two budgets, this production is compensated by a substantial elevation of dissipation, while in the case of the shear stress, the increased (negative) production is compensated by a reversal of the pressure-velocity-interaction term from a negative to a positive level. In the absence of wall shear, production is low at the wall, but not zero, because of a minor streamwise contribution. Hence, in the budgets of k and $\overline{uu}$, the near-wall dissipation is also reduced. However, the reduction is moderate, and there is still a near-wall peak, but this is a result of increased diffusion towards the wall and an elevation of the pressure-velocity correlation. In the case of $\overline{uu}$ (and also $\overline{ww}$, as shown below) the viscous diffusion becomes negative at the shear-free wall to balance, together with dissipation, the processes of convection, turbulent diffusion and pressure-velocity correlation, a behaviour also observed by Perot and Moin [10] at an ideal free-surface.

The fact that the pressure-velocity correlation of $\overline{uu}$, negative in presence of wall-shear, exhibits a narrow positive peak very near to the wall, in the absence of shear, and then becomes negative far away from the wall, implies a very different energy-transfer mechanisms in the two flows: in the real jet, the component $\overline{uu}$ has to transfer energy to the other two components, while in absence of wall shear $\overline{uu}$ receives energy very close to the wall and transfers energy to the other two components away from the wall. In the DNS of turbulent shear below a free surface performed by Shen *et al.*, the streamwise-stress budget also exhibits a gain in energy through the pressure-velocity correlation in the layer located very close to the surface, while in the shear layer away from the wall, $\overline{uu}$ transfers energy to $\overline{vv}$ and to $\overline{ww}$, as is the case in any free shear flow. More details on the mechanism of turbulence-energy redistribution will be given in section 3.5 by considering, separately, the non-deviatoric, and thus redistributive, part of the pressure-velocity correlation.

One common feature shared by both flows is the importance of turbulent transport from the outer layer towards the wall, which reflects the strong interaction between the outer shear layer and wall. This is especially prominent in the budgets of $\overline{vv}$. Although this stress is not dynamically active, it is of critical importance to the behaviour of $\overline{uv}$ and hence, indirectly, to that of the mean flow. The high level of turbulent diffusion is also noticeable in the budgets of $\overline{uv}$. In fact, in the presence of wall shear, this process is responsible for the displacement of the zero-shear-stress and shear-strain positions, and for the existence of a very limited log-law region (see Dejoan and Leschziner [2]). In the absence of wall shear, shear-stress diffusion is high and compensated by a negative pressure-velocity correlation. In contrast, in the presence of wall shear, this correlation is forced to become positive to compensate, in combination with turbulent diffusion, the strong negative production.

A striking difference between the two budgets of $\overline{vv}$ arises from the role of the pressure-velocity correlation. In both flows, production is virtually negligible, and stress diffusion towards the wall from the outer shear layer is the dominant positive contributor to the stress close to the wall. In the presence of wall shear, the turbulent transport of $\overline{vv}$ is compensated mainly by dissipation and a slight negative near-wall peak of pressure-velocity correlation. This latter behaviour is not observed in a standard boundary layer, where turbulent transport is low and the pressure-velocity correlation is observed to be positive. The low (and negative) level of the pressure-velocity correlation is related to the high gain by turbulent transport. In absence of wall shear, this latter process appears to be amplified: the much higher input of stress diffusion is compensated by a much higher negative peak of the pressure-velocity correlation, with dissipation increasing only slightly, although, very close to the wall, the dissipation features a weak negative peak to balance the increase in viscous transport. This suggests significant differences in the mechanism of near-wall damping of the wall-normal stress between the two flows. In the near-wall region of the zero-wall-shear jet, the peak of turbulent transport is higher and located closer to the wall. In presence of wall shear, in contrast, turbulent transport is damped by viscous effects in the near-wall region, which explains the lower level of pressure-velocity correlation. However, for both flows, this correlation becomes positive for distances from the wall $y/y_{1/2} > 0.1$, indicating a reverse transfer of energy as the outer layer is approached, characteristic of any free-shear layer.

One important feature to highlight, by reference to the zero-crossings of turbulent transport and the position of the peak diffusion, is the deeper penetration of the outer layer into the wall region when there is no wall shear. This may be associated with the substantial structural differences in the near-wall turbulence of the two flows: in the absence of wall shear, the near-wall layer is populated with large-scale eddies, which are more effective in transporting turbulence towards the wall. This is consistent with the observations of structural features, discussed in section 3.3, which reveal that, in the absence of shear, large eddies migrate towards the wall and splat strongly onto it. In contrast, in the presence of wall shear, the near-wall region is populated with small-scale eddies, which tend to act as a "shield", inhibiting the splatting of the large eddies onto the wall itself.

As regards $\overline{ww}$, the budgets for the two jets are similar, one difference being the higher level of pressure-velocity correlation in presence of wall shear, reflecting a strong gain at the expense of the two other stress components. Another difference is that, in absence of wall shear, convection is substantially higher, and this is associated with the higher near-wall level of $\overline{ww}$ combined with the maximum streamwise velocity at the inviscid wall. The dissipation of $\overline{ww}$ is not greatly affected by the presence of shear, except very close to the wall, where the stress has to be driven towards zero by viscous action.

3.5 Non-deviatoric pressure term and energy redistribution

As noted earlier, the role of the pressure-velocity correlation, Π_{ij}, near the wall differs greatly for the two flows. Conventionally, especially in the context of statistical modelling, this term is decomposed into non-deviatoric and deviatoric fragments, each held to play a different physical role. The implications arising from different decompositions form the subject of this section.

It is noted first that the non-deviatoric term, Φ_{ij}, differs from the pressure-velocity interaction, Π_{ij} , through the inclusion of pressure transport in the latter. This fragment can be of major importance near the wall, in contrast to the assumption that it can be ignored made in most forms of second-moment closure. In incompressible conditions, $\Phi_{kk} = 0$, and the non-deviatoric term acts as a redistributor of turbulence energy among the normal stresses. The most commonly used decomposition, referred to as "classical" below, is:

$$\begin{aligned} \Phi_{ij} &= \overline{\frac{p}{\rho}\left(u_{i,j} + u_{j,i}\right)} \\ d^p_{ij} &= -\left[\overline{\frac{p}{\rho}\left(u_i\delta_{kj} + u_j\delta_{ki}\right)}\right]_{,k} \end{aligned} \tag{2}$$

where Φ_{ij} is the pressure-strain correlation and d^p_{ij} is the pressure diffusion.

However, other decompositions are possible, one being that of Mansour *et al.*, 1988 [23]:

$$\begin{aligned} \Phi_{ij} &= -\frac{1}{\rho}\left[\overline{\left(u_i p_{,j} + u_j p_{,i}\right)} - \frac{1}{\rho}\frac{\overline{u_i u_j}}{2k}\left(\overline{pu_k}\right)_{,k}\right] \\ d^p_{ij} &= -\frac{1}{\rho}\frac{\overline{u_i u_j}}{2k}\left(\overline{pu_k}\right)_{,k} \end{aligned} \tag{3}$$

which is a variation of a previously proposed decomposition by Lumley (see [24])

Here, attention focuses on the classical and Mansour's decompositions, the former having been used as a basis for approximating the pressure-velocity interaction in most second-moment closures. The closure of Craft *et al.*, [25] is one of very few schemes leaning on Mansour's decomposition. Previous studies by the present authors [4] have shown that, for the real wall jet, Lumley's decomposition leads to a non-deviatoric term close to the classical decomposition, in particular for $\overline{vv}$ and $\overline{uv}$.

Any of these decompositions makes Φ_{ij} trace free (in incompressible conditions), thus reflecting its physical role as a redistributor of the turbulence energy among the normal stresses. However, as illustrated by Figs. 22-25, the contribution of the pressure-transport term differs greatly from one decomposition to the other. A prominent feature of the classical decomposition is that the pressure diffusion balances the pressure-strain term in the near-wall region, for both jets, especially in the case of $\overline{vv}$ and $\overline{uv}$, whereas use of Mansour's decomposition renders the pressure-transport term much less important, and the non-deviatoric pressure-velocity fragment is close to the parent correlation. From a modelling point of view, this suggests that Mansour's decomposition is preferable, as it reduces substantially the need to model the pressure-transport term, which is commonly ignored or implicitly held to be included in the turbulent transport, usually modelled by way of a general gradient-diffusion hypothesis. On the other hand, a disconcerting property of the pressure transport, as defined by Eq. (3), is its non-zero value in homogeneous directions, an issue discussed by Groth [26]. The physical implications of the decompositions (2) and (3), especially in respect of physical realism, are also discussed in Speziale [27] and Kim and Chung [28]. Another conceptual drawback is that the physical processes represented by the fragments in Mansour's decomposition are somewhat more obscure than those in the classical decomposition.

Against the above background, attention focuses below on the non-deviatoric term, Φ_{ij}, as defined by (2) and (3), and a discussion is provided of the contrasting energy-redistribution processes observed in the real jet and the zero-wall-shear jet.

The profiles of Φ_{ij} shown in Figs. 22-25 bring to light the major effects of the near-wall shear on the redistribution of energy by the pressure-velocity-interaction processes. First, it is observed that both decompositions (2) and (3) are consistent, in so far as both have the same sign for the normal components of Φ_{ii}, thus giving rise to a similar redistribution pattern of turbulence energy among the normal-stress components. However, the *rate* of energy transferred implied by the two decompositions is different, depending upon the relative contributions of Φ_{ij} and d^p_{ij}. Use of (2) leads to higher values of Φ_{ij}, especially in the case of $\overline{vv}$ and $\overline{uv}$, for which Φ_{ij} almost balances d^p_{ij} very close to the wall. This balance, previously observed in fully-developed channel flows by Mansour *et al.* [23], not only applies to the real jet, but is also observed in the zero-wall-shear jet. While this implies that the balance is intrinsically linked to the wall-blocking process, it is noticeable that the distance from the near-wall layer over which this balance prevails is different in the two jets. This is seen especially clearly in the plots for $\overline{vv}$, suggesting a more far-reaching influence of the wall into the outer flow by pressure-fluctuations effects in the presence of wall shear. Here, a link can be identified to the level of near-wall anisotropy as the wall is approached. Reference to the distributions of the flatness factor, Fig. 8, have shown in section **??** that the approach to 2D turbulence start closer to the wall and proceed at a considerably higher rate in the zero-wall-shear jet relative to the real jet: the start of the steep decrease occurs at around $y/y_{1/2} \sim 0.1$ relative to 0.15. This latter value indicates that, in the real jet, the wall-blocking effects extend away from the wall region up to a depth of order 3 times the thickness of the sheared near-wall layer. The above positions are also those at which d^p_{vv} and Φ_{vv} begin to diverge as the wall is approached. If it is accepted that this divergence is indeed indicative of the depth to which $\overline{vv}$ is damped by wall-related effects, it follows that the onset of the steep upward trend of the flatness factor is a good indicator of the damping influence of the wall by pressure-fluctuations effects. To an extent, the deeper penetration in the real wall jet is expected. The viscous near-wall effects hinder the splatting process and push the pressure-strain term of $\overline{uu}$ to negative values, causing a reduction of this stress, rather than the increase observed (and anticipated) in the absence of wall shear as splatting results in energy extracted from $\overline{vv}$ being transferred to both $\overline{uu}$ and $\overline{ww}$. The splatting process is thus shifted away from the wall (compare the variations of Φ_{vv} in Figs 22 and 24 or Fig. 23 and 25), suggesting a form of "shear-sheltering".

A composite view of the energy transfer among the normal stresses is conveyed by Fig. 26 through the profiles of the pressure-strain term, defined according to the classical decomposition (2). In agreement with earlier comments, in section 3.4, Fig. 26 shows that, in the presence of wall shear, energy is being transferred in the near-wall region from $\overline{vv}$ *and* $\overline{uu}$ to $\overline{ww}$, whereas, in the absence of shear, very close the wall, energy is being transferred from $\overline{vv}$ to *both* $\overline{uu}$ and $\overline{ww}$. This redistribution is not symmetric, however, reflecting the influence of the outer shear layer on the region adjacent to the zero-shear wall. In the absence of such shear, the redistribution would be expected to be symmetric. When wall shear is added, the component $\overline{uu}$ is mainly produced by shear strain, and this mechanism is so strong that energy has to be removed from $\overline{uu}$ to $\overline{ww}$. In absence of wall shear, the turbulent motions of the outer layer "splat" on the wall, and energy is transferred from the wall-normal stress to the wall-parallel components.

Fig. 26 shows that, in the presence of shear, the pressure-strain term of $\overline{vv}$ remains negative over a larger distance from the wall than in the absence of near-wall shear. This implies a more far-reaching influence of the wall on the outer layer and a higher level of anisotropy, previously suggested already by reference to the profile of the flatness parameter A. This supposition is given further support by the higher level of anisotropy in the dissipation rate in the presence of shear, as seen in the budgets of $\overline{uu}$, $\overline{vv}$ and $\overline{ww}$.

It is pertinent to examine here to what extent some of the processes highlighted above have been observed in previous studies. In their DNS of grid-decaying turbulence passing over a moving wall, Perot and Moin [10] argue that the inter-component energy transfer near the wall is governed by "splat" and "anti-splat" events, the imbalance between the two resulting in inter-component energy transfer, which is controlled by viscous processes associated with dissipation and diffusion. Perot and Moin observe that, near an idealized free surface, viscous effects are small, and therefore energy redistribution is low too. In contrast, the present results show that, especially in the case of the zero-wall-shear jet, the redistributive pressure-velocity correlation makes an important contribution to the stress budgets, in particular in the case of $\overline{vv}$, for which it balances the large input of turbulent transport (see Fig. 19). Thus, the present zero-shear-wall jet is very different in terms of the near-wall processes, and – adopting the terminology of Perot and Moin – the results imply a strong imbalance between "splats" and "anti-splats". The zero-wall-shear jet is characterized by an especially high level of turbulent diffusion from the outer sheared flow towards the wall, as seen from Fig. 19, and this is enhanced by the strong undamped splatting at the shear-free wall, reflected by the strongly elevated near-wall pressure-velocity interaction.

Features similar to the present pattern of energy-redistribution processes have also been identified by Handler *et al.* [11], Lam and Banarjee [13], Kuroda *et al.* [15] and Shen *et al.* [16] in open-channel flow and in the related case of a free surface above a shear flow, in both of which the inter-component energy transfer is also substantial. However, in these studies, the turbulent transport was relatively small. Thus a distinctive message derived from the present study is that turbulent stress diffusion towards the wall, especially of $\overline{vv}$, is a major mechanism responsible for controlling the near-wall redistribution process and thus the precise details of the blocking effect of the wall on the stresses. These observations may be claimed to have important modelling implications. Within the framework of second-moment closure, one obvious requirement is that stress diffusion needs to be modelled realistically. Another implication is that the redistribution (or pressure-strain) process needs to be sensitized to the near-wall shear in such a way that the effects of the shear on the redistribution process well beyond the actual near-wall-shear region are correctly accounted for. This thus appears to call for a "non-local" approximation with "elliptic" features associated with the propagation of pressure fluctuations.

3.6 Integral length scales

For the real wall jet, Dejoan and Leschziner [2] demonstrate, by reference to DNS results for channel flow, that the length scale in the near-wall region is strongly elevated relative to the equilibrium value, reflecting the "migration" of large-scale eddies from the outer shear layer towards the wall. This is thus highlighted as one important aspect of the interaction between the outer shear layer and the wall layer. Here, Fig. 27 contrasts the variations of the integral length scale $l_\varepsilon = k^{3/2}/\varepsilon$, normalised by $y/y_{1/2}$ and the equilibrium length scale $C_\mu \kappa y$ for the two jets (where $\kappa = 0.45$ and $C_\mu = 0.09$). The main message conveyed by the comparison is that, in the absence of shear, the length scale experiences a further massive increase in the near-wall region. This increase thus supports the notion of a wall-directed migration of eddies, referred to earlier. In the presence of shear, the boundary layer generates a range of scales which are considerably smaller than those in the absence of wall shear - the difference being conveyed well in Fig. 10. These eddies depress the integral scale as the wall is approached, reflecting an interpenetration of the two scale ranges. However, the influence of the outer-layer scales is very strong, and this causes the outer eddies to substantially elevate the length scale in the boundary layer, relative to the equilibrium level, right down to the wall, through the large input of turbulence energy by diffusion.

4 Conclusions

The study set out to juxtapose two types of wall jet, in one of which wall shear is synthetically nullified, so as to replace the real wall by a flat shear-free surface. The objective was to differentiate between the effects of wall-blocking and near-wall shear on the statistical and structural properties of the wall jet.

One important conclusion emerging from the study is that the near-wall region is affected by the wall to a depth that exceeds substantially – by a factor of about 3 – the thickness of the sheared near-wall layer. In the absence of wall shear, the depth is somewhat lower, about two thirds of that in the real wall jet. This points unambiguously to the wall-blocking process and to non-local effects arising from pressure fluctuations and their reflection being the cause. However, the manner in which the pressure fluctuations affect the statistical state of the flow near the wall is strongly modified by the presence or absence of shear.

While in both flows, near-wall (or near-surface) anisotropy is very high, the details of the anisotropy differ significantly. In the absence of shear, the anisotropy arises principally from energy being extracted by pressure-velocity interaction from the wall-normal component $\overline{vv}$ and being diverted to the wall-parallel components. However, this redistribution is not quite symmetrical, and this reflects the influence of shear in the outer layer on the near-wall processes, notably by turbulent diffusion towards the wall. In contrast, in the presence of shear, energy is being extracted from both $\overline{vv}$ and $\overline{uu}$ and diverted preferentially to the streamwise component $\overline{ww}$. Hence, the transfer of energy from $\overline{vv}$ to $\overline{uu}$ is impeded by the presence of wall shear. This difference is mainly associated with the structural properties of the near-wall region. In the absence of wall shear, the eddies migrating towards the wall are flattened by the surface, through "splatting", in a broadly isotropic manner parallel to the wall. The addition of shear leads to a higher level of anisotropy due to the wall-shear generation of streamwise-velocity fluctuations, which is reflected by the characteristic near-wall streaky structures.

Significantly, the flatness parameter, representing the norm of the anisotropy in a scalar sense, is only slightly sensitive to the absence or presence of wall shear, and is shown (also by reference to the pressure-strain profiles) to be a good indicator, in both flows, of the distance from the wall over which wall-blocking is effective. While the implication is thus that this parameter may be exploited in statistical closures to represent the overall effects of the wall, it does not allow the interactive effects of near-wall shear and wall-blocking to be characterised separately.

A distinctive and influential transport process in both jets, identified by the budgets, is turbulent diffusion by triple correlations. This process is particularly important in the case of the wall-normal stress $\overline{vv}$, tending to increase the stress and being compensated by dissipation and pressure-velocity interaction. In the absence of shear, this mode of transport is especially strong, and this is indicative of the unimpeded penetration of large-scale eddies towards the wall - a process that is also characterised by eddy length scales which, in the case of zero shear, hardly diminish as the wall is approached. While the interplay is modulated by near-wall shear, it is clear that over a substantial proportion of the interaction layer, beyond $y/y_{1/2}$=0.05, the effects of the wall are not only influenced by the viscous effects associated with the near-wall shear, but also by the transport associated with the triple correlations. Especially in the absence of wall shear, it is the high level of turbulent diffusion of $\overline{vv}$ that balances the pressure-velocity interaction, which causes an energy depletion in the wall-normal component. The effect of diffusion is less prominent in the budgets of the other stress components, but remains influential in the interaction region, especially in the case of the shear stress.

Close to the wall, visualisations show that the two jets feature very different structural properties. As noted already, in the presence of shear, the structure is dominated by fine and elongated streaks generated by the high wall shear. In contrast, in absence of wall shear, the near-wall structure is characterised by much larger, more "isotropic" features. However, beyond the immediate sheared near-wall layer, the structural properties of the real and wall-shear-free jets differ little. An impression conveyed by visualisation is that the near-wall shear layer acts as a "shield" against the penetration of large-scale vortices migrating towards the wall. Consistently, there is a precipitous drop in the integral length scale as the wall is approached in the presence of shear. However, the length scale remains substantially higher than the level implied by equilibrium, and this reflects, again, the role of turbulent diffusion in the balance of processes close to the wall.

5 Acknowledgements

This study was supported financially by the UK Science and Engineering Research Council (EPSRC). The computations were performed on the Origin 3800 computer at the national CSAR service in Manchester, using resources provided as part of the EPSRC grant.

References

[1] A. Dejoan and M.A. Leschziner. LES studies on the correspondance between the interaction of shear layers in post-reattachment and in a plane turbulent wall jet. Accepted for publication in *Direct and Large-Eddy Simulation VI*, Editors: E. Lamballais,R. Friedrich, B. J. Geurts, O. Métais, Springer Verlag, 2006.

[2] A. Dejoan and M.A. Leschziner. Large eddy simulation of a plane turbulent wall jet. *Phys. Fluids*, 17, 025102, 2005.

[3] A. Dejoan and M.A. Leschziner. LES study of the statistical characteristics of the plane turbulent wall jet. *Proceedings of the Tenth European Turbulence Conference, H.I Andersson and P.-A. Krögstad (Eds)*, pages 663–666, 2004.

[4] A. Dejoan, C. Wang and M.A. Leschziner. Assessment of turbulence models for predicting the interaction region in a wall jet by reference to LES solution and budgets. *ETMM6, Sardinia, Italy*, pages 97–106, 2005. Accepted for publication in *Flow, Turbulence and Combustion*.

[5] J. Hunt and J. Graham. Free stream turbulence near plane boundaries. *J. Fluid Mech.*, 84(2):209–235, 1978.

[6] T. Uzcan and W. Reynolds. A shear-free turbulent boundary layer. *J. Fluid Mech.*, 28(4):803–821, 1967.

[7] S. M. Thomas and P. E. Hancock. Grid turbulence near a moing wall. *J. Fluid Mech.*, 82(3):481–496, 1977.

[8] S. Biringen and W. Reynolds. Large-Eddy-Simulation of the shear-free turbulent boundary layer. *J. Fluid Mech.*, 103:53–63, 1981.

[9] D. Aronson, A. V. Johansson, and L. Löfdhal. Shear-free turbulence near a wall. *J. Fluid Mech.*, 338:363–385, 1997.

[10] B. Perot and P. Moin. Shear-free turbulent boundary layers. part 1. Physical insights into near-wall turbulence. *J. Fluid Mech.*, 295:199–227, 1995.

[11] R. A. Handler, T. F. Swean Jr, R. I. Leighton and J. D. Swearingen. Length scales and the energy balance for turbulence near a free surface. *AIAA Journal*, 31(11):1998–2007, 1993.

[12] M. Rashidi and S. Banarjee. The effect of boundary conditions and shear rate streak formation and breakdown in turbulent channel flow. *Phys. Fluids A*, 2:1827–1838, 1990.

[13] K. Lam and S. Banarjee. On the condition of streak formation in bounded turbulent flow. *Phys. Fluids A*, 4:306–320, 1992.

[14] Y. Pan and S. Banarjee. A numerical study of free-surface in channel flow. *Phys. Fluids A*, 7:1649–1664, 1995.

[15] N. Kasagi A. Kuroda and M. Hirata. Direct numerical simulation of turbulent plane couette-poiseuille flows: effect of mean shear on the near wall turbulence structures. *Ninth Symposium on "Turbulent shear flows", Kioto, Japan, August 16-18*, 8:4–1–4–6, 1993.

[16] L. Shen, X. Zhang, D. K. P. Yue and G. S. Triantafyllou. Surface layer for free-surface turbulent flow. *J. Fluid Mech.*, 386:167–212, 1999.

[17] J. G. Eriksson, R. I. Karlsson and J. Persson. An experimental study of a two-dimensional plane turbulent wall jet. *Experiments in Fluids*, 25:50–60, 1998.

[18] J. Eriksson. Experimental studies of the plane turbulent wall jet. *Ph.D. Thesis, Royal Institute of Technology. Department of Mechanics, Stockolm, Sweden*, 2003.

[19] H. Schlichting. Boundary layer theory. *Springer Verlag; 8th edition*, 1999.

[20] M. Germano, U. Piomelli, P. Moin and W. Cabot. Dynamic subgrid-scale eddy viscosity model. *Phys. Fluids A*, 3:1790, 1991.

[21] J. Kim M. J. Lee and P. Moin. Structure of turbulence at high shear rate. *J. Fluid Mech.*, 216:561–583, 1990.

[22] J. Jiménez and A. Pinelli. The autonomous cycle of near-wall turbulence. *J. Fluid Mech.*, 389:335–359, 1999.

[23] N. N. Mansour, J. Kim and P. Moin. Reynolds-stress and dissipation-rate budgets in a turbulent flow. *J. Fluid Mech.*, 194:15–44, 1988.

[24] L. Lumley. Pressure-strain correlation. *Phys. Fluids*, 18:750, 1975.

[25] T. J. Craft and B. E. Launder. A Reynolds stress closure designed for complex geometries. *Int. J. Heat and Mass Transfer*, 17:245–254, 1996.

[26] J. Groth. Description of the pressure effects in the Reynolds stress transport equations. *Phys. Fluids A*, 3 (9):2276–2277, 1991.

[27] C. G. Speziale. Modeling the pressure gradient-velocity correlation of turbulence. *Phys. Fluids*, 28:69–71, 1985.

[28] S. K. Kim and K. Chung. Spatial transport of Reynolds stresses by pressure fluctuations. *Phys. Fluids*, 6 (11):3507–3509, 1994.

List of Figures

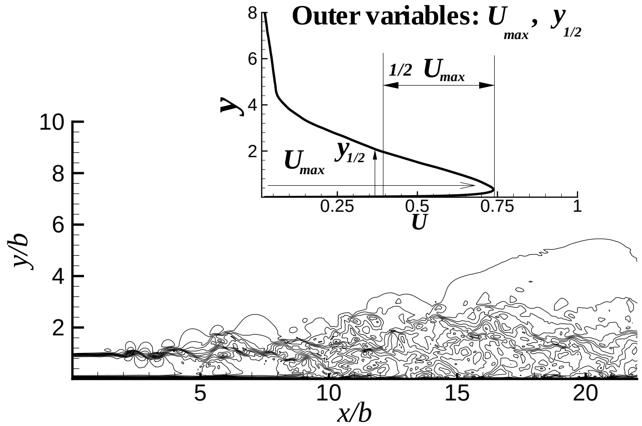

Figure 1: Wall-jet geometry.

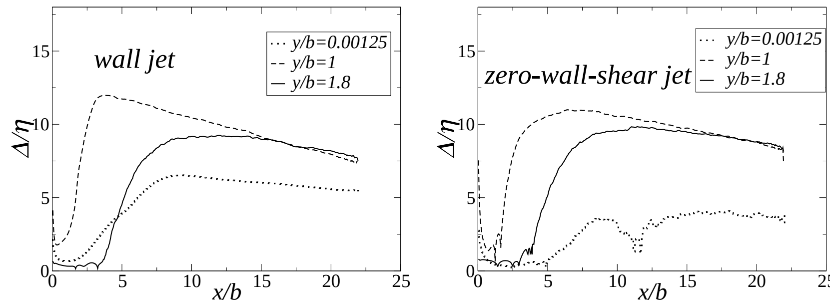

Figure 2: Ratio of the grid size to the Kolmogorov length scale given at different locations.

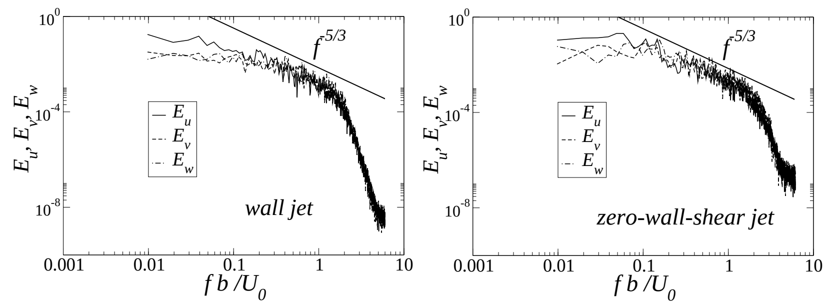

Figure 3: Frequency spectra given at $x/b = 20$, $y/b = 1$.

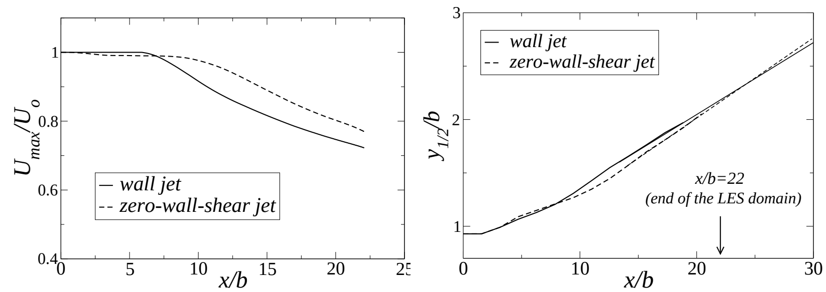

Figure 4: Left: decay of the maximum streamwise velocity. Right: spreading rate.

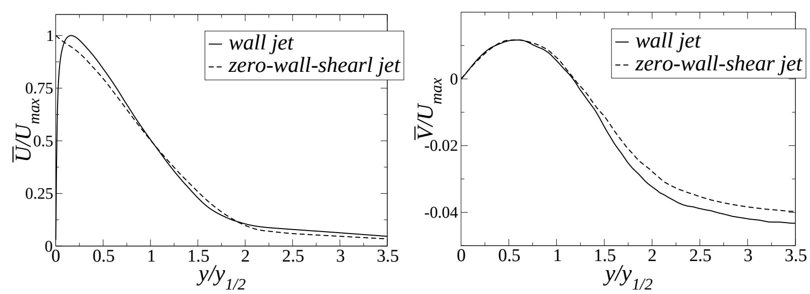

Figure 5: Mean streamwise and wall-normal velocity profiles at the location $x/b = 20$.

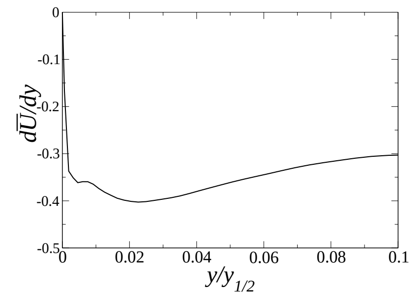

Figure 6: Zero-wall-shear jet: $\partial\overline{U}/\partial y$ profile at the location $x/b = 20$ normalised by the outer scale U_{max} and $y_{1/2}$.

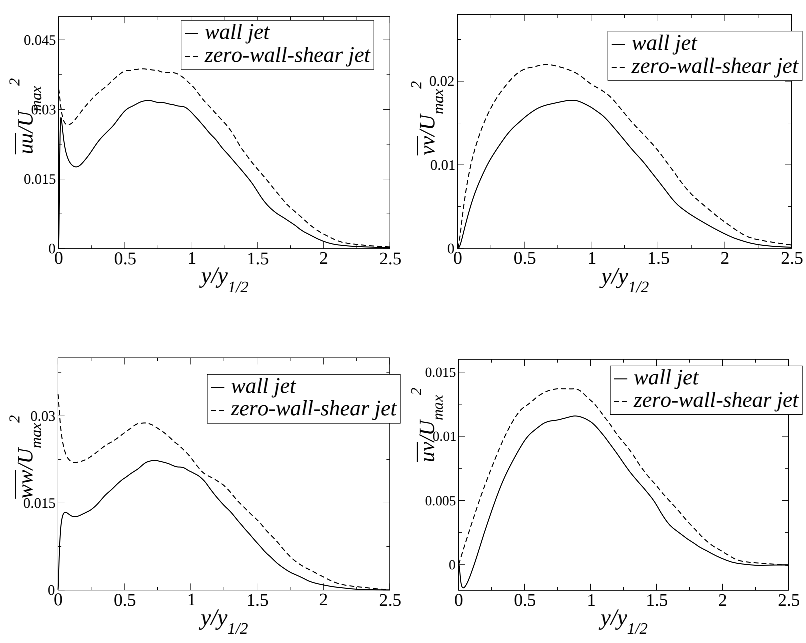

Figure 7: Profiles of Reynolds-stress components at the location $x/b = 20$.

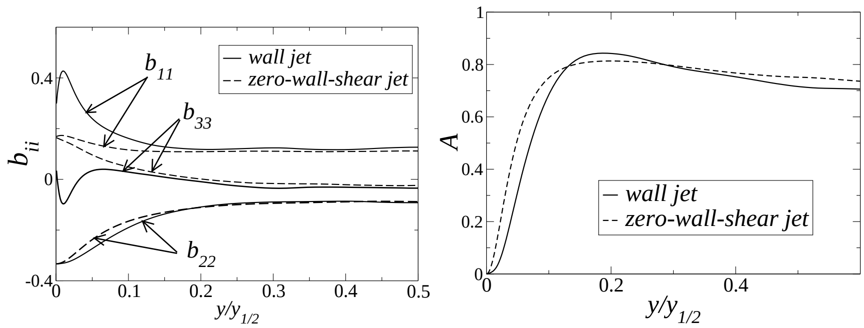

Figure 8: Anisotropy normal stresses profiles (left) and flatness profiles (right) at the location $x/b = 20$.

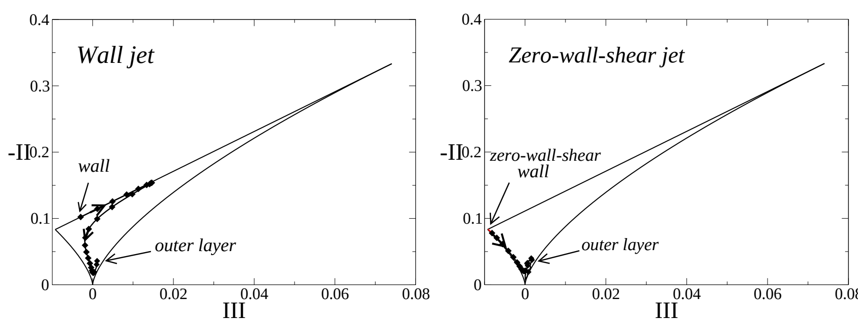

Figure 9: Anisotropy maps at the location $x/b = 20$.

Figure 10: Contours of instantaneous streamwise velocity fluctuations, u/U_o, parallel to the wall at $y/y_{1/2} \sim 0.02$. The plot contains 40 contours of u/U_o in the range [-1.5:1.5]. Top: real wall jet. Bottom: zero-wall-shear jet

Figure 11: Contours of instantaneous streamwise velocity fluctuations, u/U_o, parallel to the wall at $y/y_{1/2} \sim 0.4$. The plot contains 40 contours of u/U_o in the range [-1.5:1.5]. Top: real wall jet. Bottom: zero-wall-shear jet

Figure 12: Instantaneous field of transverse motion, $(w/U_o, v/U_o)$ in the cross-flow plane at $x/b = 17$. Top: real wall jet. Bottom: zero-wall-shear jet

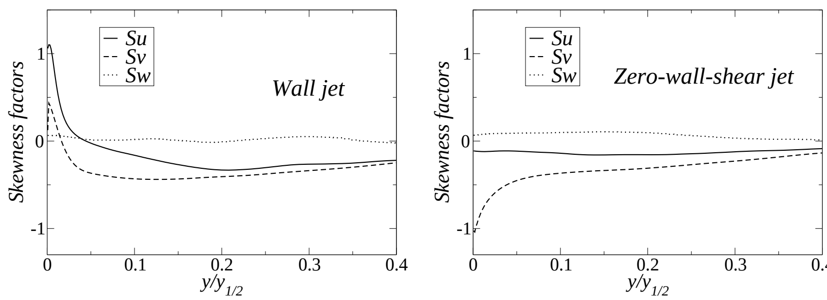

Figure 14: Skewness factors at the streamwise location $x/b = 20$.

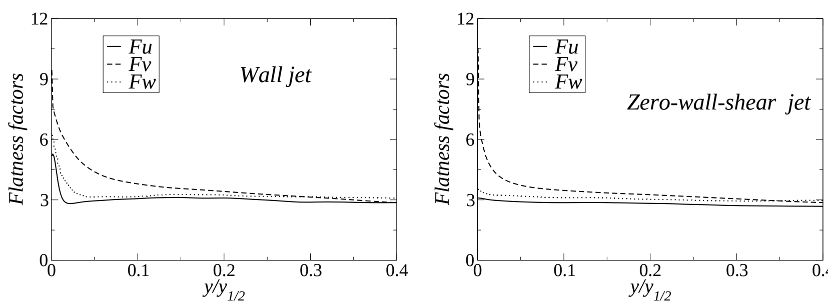

Figure 15: Flatness factors at the location $x/b = 20$.

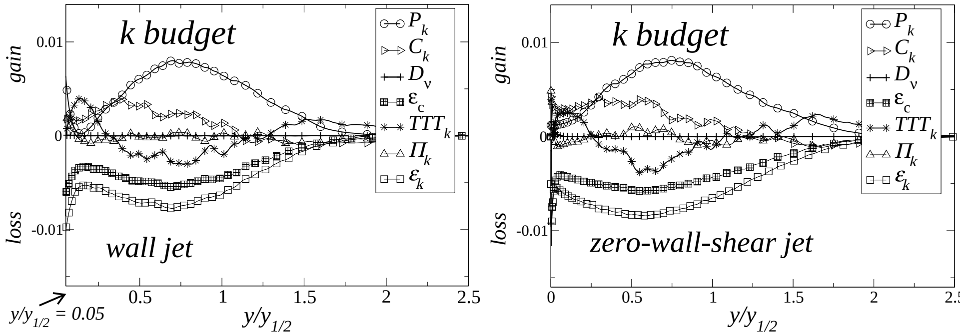

Figure 16: Budgets of the kinetic energy at the location $x/b = 20$, in the outer region. Normalised by $U_{max}^3/y_{1/2}$. See Eq. (1) for symbols definition.

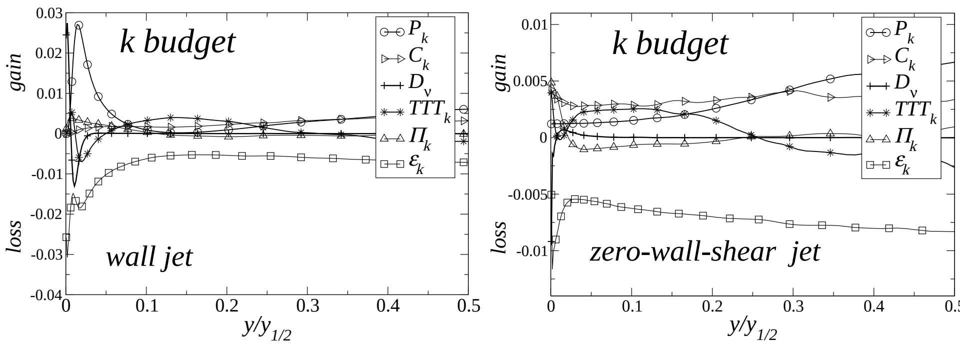

Figure 17: Budgets of the kinetic energy at the location $x/b = 20$, in the near-wall region. Normalised by $U_{max}^3/y_{1/2}$. See Eq. (1) for symbols definition.

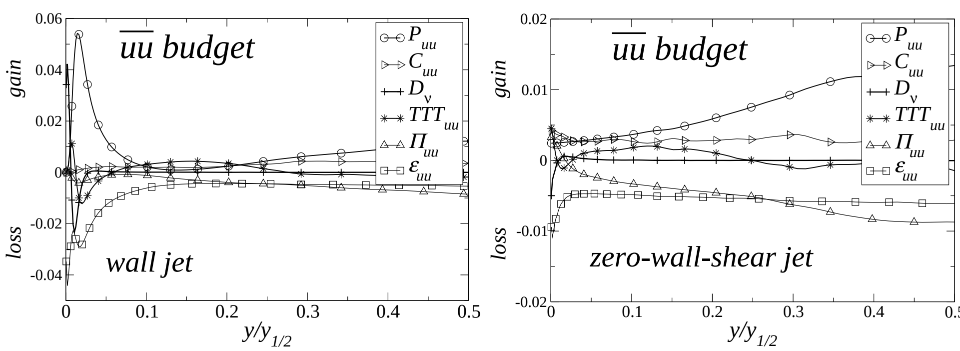

Figure 18: Budgets of the $\overline{uu}$ stress at the location $x/b = 20$, in the near-wall region. Normalised by $U_{max}^3/y_{1/2}$. See Eq. (1) for symbols definition.

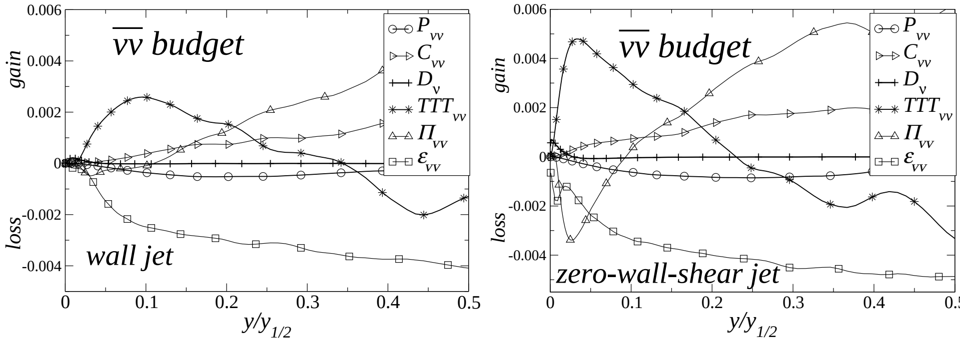

Figure 19: Budgets of the $\overline{vv}$ stress at the location $x/b = 20$, in the near-wall region. Normalised by $U^3_{max}/y_{1/2}$. See Eq. (1) for symbols definition.

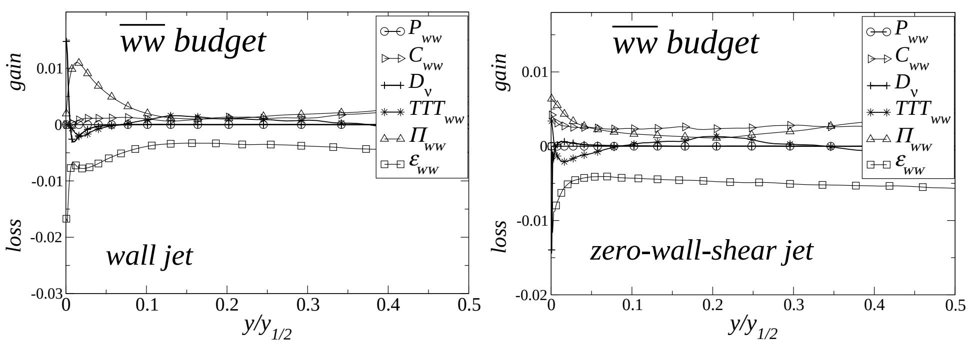

Figure 20: Budgets of the $\overline{ww}$ stress at the location $x/b = 20$, in the near-wall region. Normalised by $U^3_{max}/y_{1/2}$. See Eq. (1) for symbols definition.

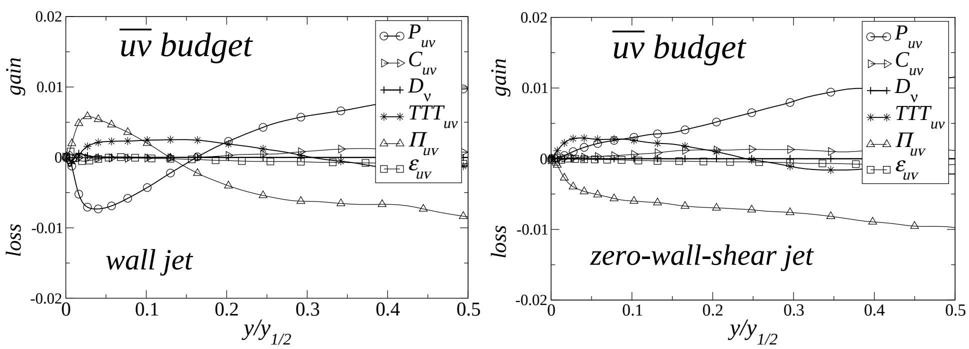

Figure 21: Budgets of the $\overline{uv}$ stress at the location $x/b = 20$, in the near-wall region. Normalised by $U^3_{max}/y_{1/2}$. See Eq. (1) for symbols definition.

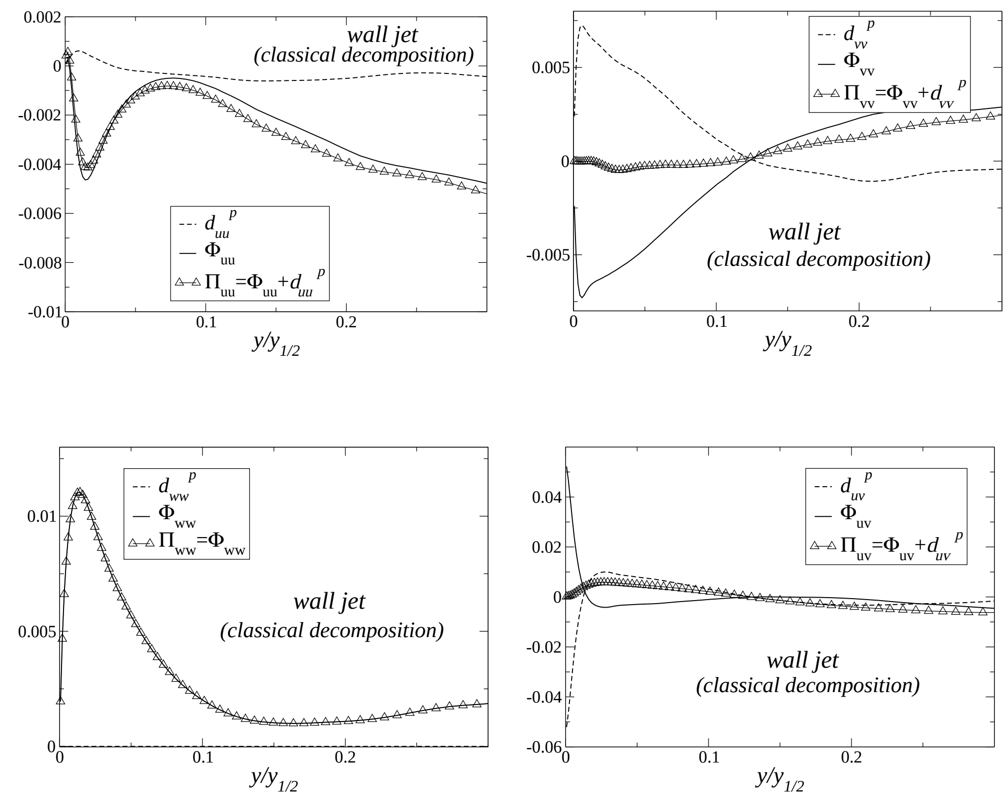

Figure 22: Real jet: classical decomposition of the velocity-pressure correlation

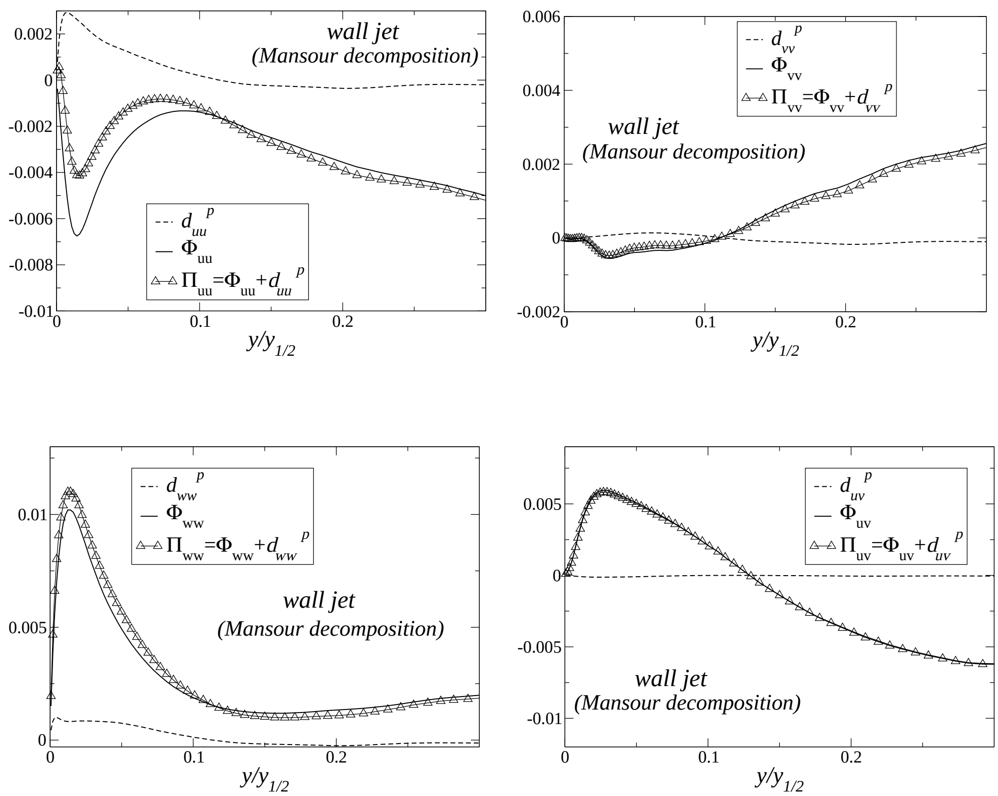

Figure 23: Real jet: Mansour's decomposition of the velocity-pressure correlation

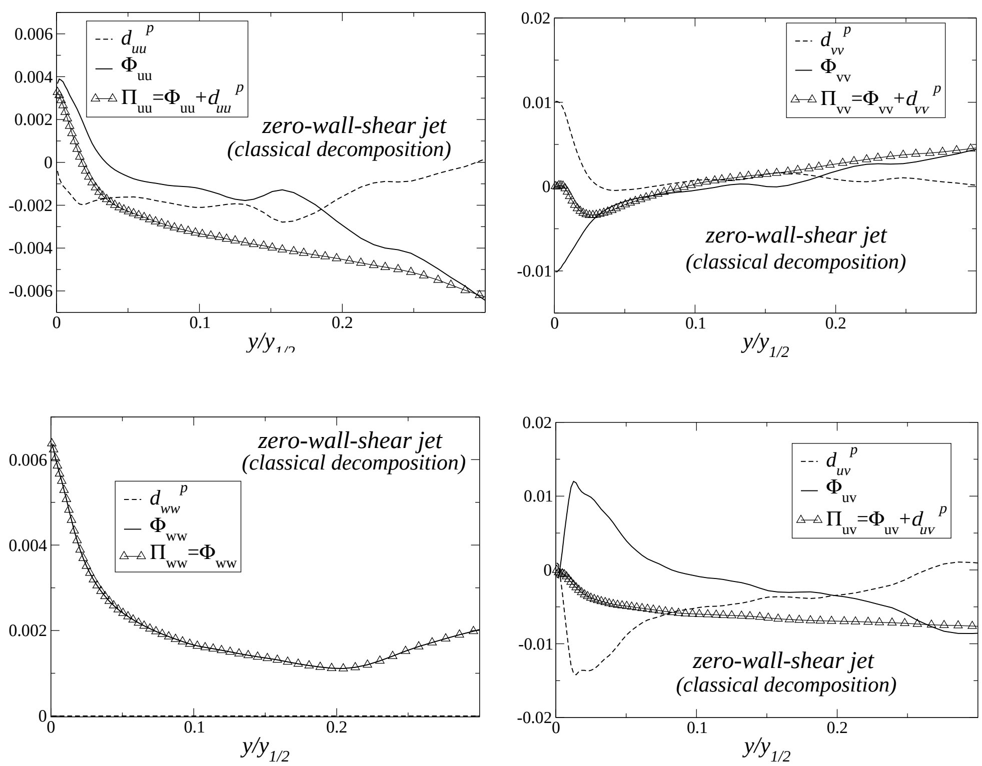

Figure 24: Zero-wall-shear jet: classical decomposition of the velocity-pressure correlation

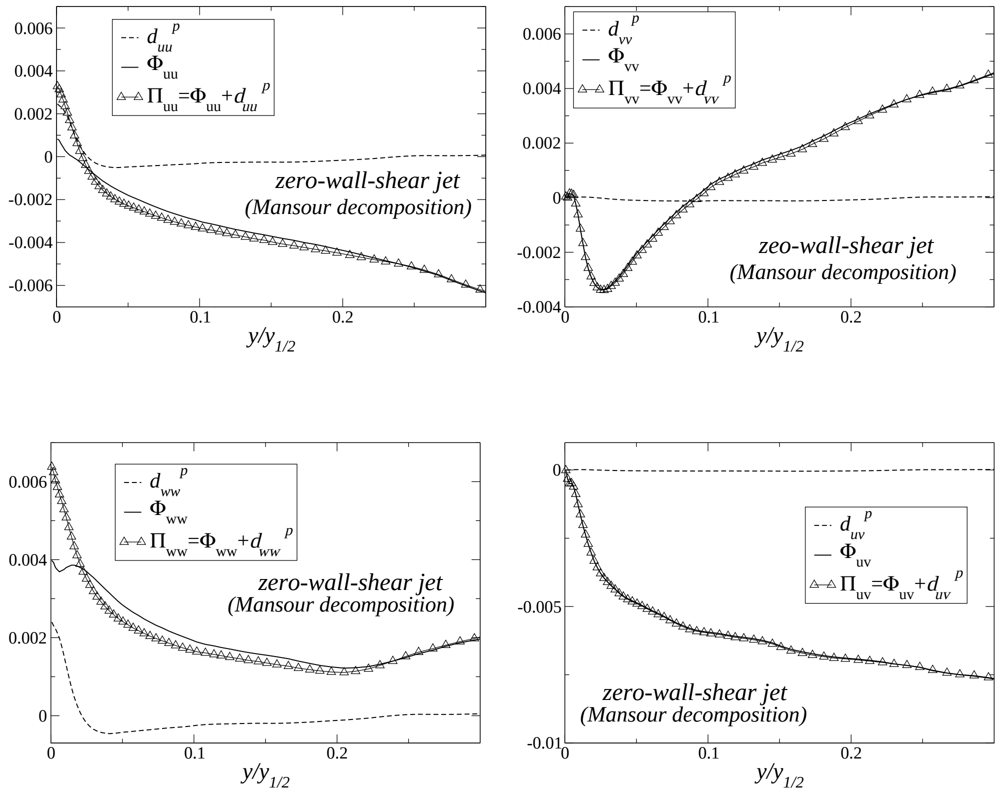

Figure 25: Zero-wall-shear jet: Mansour's decomposition of the velocity-pressure correlation

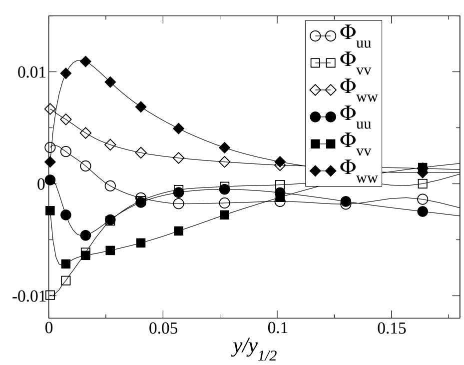

Figure 26: Wall and zero-wall-shear jet: comparison of the energy redistribution through the pressure-strain term decomposed according to the classical decomposition.

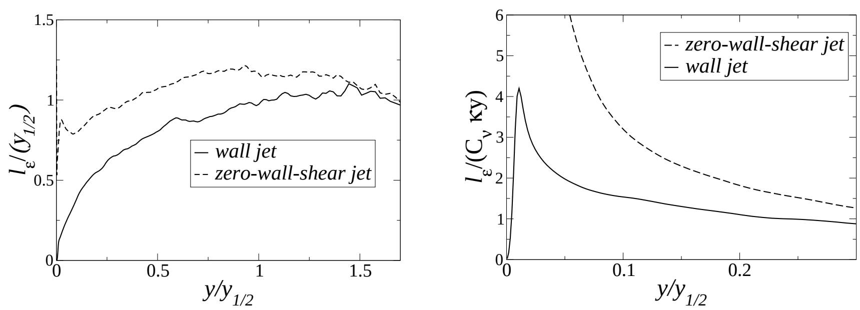

Figure 27: Integral length scale, $l_\varepsilon = k^{3/2}/\varepsilon_k$ at the location $x/b = 20$. Left: normalised by $y_{1/2}$. Right: normalised by the equilibrium length scale